Ecological Indicators 150 (2023) 110231

Contents lists available at ScienceDirect

Ecological Indicators

journal homepage: www.elsevier.com/locate/ecolind

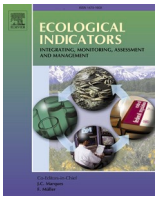

Further exploring the driving mechanism of ecological carrying capacity changes at the urban agglomeration level

Chang Liu [a,b], Tianhua Ni [a,*]

[a] School of Geography and Ocean Science of Nanjing University, Nanjing 210023, China
[b] Department of Earth and Environmental Sciences of Katholieke Universiteit Leuven, Leuven 3000, Belgium

ARTICLE INFO

Keywords:
Ecological carrying capacity
Human activities
Driving mechanism
Deep learning
Yangtze river delta urban agglomeration

ABSTRACT

The regional ecological carrying capacity (ECC) has been proposed to be strongly affected by human activities. However, the key drivers and driving patterns of ECC, especially among different regions, still lack deep understanding. The Yangtze River Delta urban agglomeration (YRDUA) is the most economically developed area facing increasing ecological pressure in China, with numerous spatial differences at the same time. In this study, the ecological footprint was used to assess ECC in the YRDUA and 40 city-level deep learning models were contructed to predict ECC according to 11 socioeconomic factors. Then, through model decomposition, independent driving effect curves were obtained, and the inner driving mechanism of the ECC evolution of each city was analyzed and classified. The results indicate that (1) "Population density" was the most significant ECC driver, while "GDP" and "Output Value of the 1st, 2nd, and 3rd Industries" were also relatively significant; (2) There were 4 types of cities whose ECC were driven by urban expansion, green economy, industry structure, and population density, respectively; and (3) Jiangsu and Anhui provinces should focus on industrial structure optimization or vegetation restoration in the future, while Shanghai and Zhejiang provinces should reduce resource and environmental costs or control population increases.

1. Introduction

Worldwide attention is now increasingly paid to the concept of sustainable development (Olawumi and Chan, 2018; Annan-Diab and Molinari, 2017; Butlin, 1989). Although the escalation in industrialization along with the acceleration of economic growth has been found in several regions, we are facing an increasing number of issues about how to maintain urban sustainability (Zhang et al., 2021). In addition, further increasing pressure on human activities risks causing widespread and irreversible changes to the earth system processes, which may threaten global development and even human race survival (Zhang et al., 2021; Griggs et al., 2013). Hence, measuring, assessing, analyzing, and predicting the regional ecological carrying capacity which is closely related to sustainability has emerged as a key issue among policymakers, researchers, and the public (Čuček et al., 2012).

The ecological footprint (EF) is a consensus indicator of the human use of environmental resources and is widely used for ecological carrying capacity (ECC) assessments (Syrovátka, 2020). This concept was first proposed in 1992 by two Canadian ecologists, Wackernagel and Rees, and developed in 1996 (Rees, 1996; Williams and Wackernagel, 1998). EF measures the demand for natural capital, which can be defined as the aggregate area of various ecologically productive lands and aquatic ecosystems (Ahmed et al., 2019; Wackernagel and Rees, 1997), while available biocapacity (BC) is the supply of natural capital. To explore the regional ecological budget, the supply (BC) and demand (EF) may be compared, and the so-called "ecological deficit" and "ecological remainder" were introduced to measure the regional ecological carrying status (Hong et al., 2007; Monfreda et al., 2004). Niccolucci et al. (2009) then proposed a 3-dimensional perspective of EF, using the ratio of EF to BC to express the intensity component regarding the depletion of natural capital stocks, which was called footprint depth.

Numerous studies on EF have been carried out since the 1970s, which can be mainly divided into ECC assessment and socioeconomic driver identification. The current ECC assessment using EF has been relatively well developed, and the scope of the research area covered different geographical regions, different scales, and even different industries, as well as a variety of natural elements (Sarkodie, 2021; Destek and Sarkodie, 2019; Lin et al., 2018; Borucke et al., 2013; Ewing et al., 2012; Wackernagel et al., 1999a,b). Globally, more than 150 countries

* Corresponding author.
E-mail addresses: chang.liu1@kuleuven.be (C. Liu), thni@nju.edu.cn (T. Ni).

https://doi.org/10.1016/j.ecolind.2023.110231
Received 10 July 2022; Received in revised form 26 March 2023; Accepted 6 April 2023
Available online 10 April 2023

are calculating their EF accounts (Galli et al., 2014). In recent years, studies on EF estimation have moved toward smaller scales, longer time series, and a more specific focus on industries and resources (Balsalobre-Lorente et al., 2019; Čuček et al., 2012; Johannesson et al., 2020; Liu et al., 2020b). More in-depth studies on EFs have started to focus on their socioeconomic drivers, but the explanation and understanding of their underlying driving mechanisms remain inadequate. Most of the studies use classical mathematical and statistical methods, such as partial least squares (PLS) regression methods (Danish et al., 2020; Yang et al., 2018), GeoDetector (Chen et al., 2020a; Pei et al., 2021), principal component analysis (PCA) (Cano-Orellana and Delgado-Cabeza, 2015) and multiple regression models (Dietz et al., 2007; Yang et al., 2022), which can only identify the key socioeconomic drivers or differentiate their significance but cannot quantify the driving mechanisms in greater detail. For example, Baabou et al. (2017) measured the EF of 19 coastal cities in the Mediterranean region, and after statistical analysis, it was found that the EF of the region is mainly contributed by food consumption, transportation, and consumption of manufactured products, whereas the differences among the EFs of different cities are mainly influenced by disposable income, level of infrastructure development, and cultural practices. Omoke et al. (2020) analyzed the ecological footprint of Nigeria from 1971 to 2014 using a nonlinear regression model and found that economic growth, energy consumption, urbanization, and economic globalization are the main drivers affecting local sustainable development. Hence, it could be noted that most of the existing studies can identify the key drivers with a significant impact on EF and discuss the positive and negative effects of relevant factors to a certain extent. Nevertheless, due to the shortage of classical research methods in the quantitative description of driving mechanisms and processes, the conclusions obtained are still relatively unquantified, and there are obvious limitations in exploring the continuity, inflection points, and synergies of their socioeconomic driving mechanisms simulation. In addition, the relationship between the driving mechanism of ecological carrying status and the variability of different regions or cities in terms of scale and economic growth patterns has received little attention, limiting the effectiveness of relevant research in supporting realistic regional sustainable development decisions.

As a rising and leading machine learning method, deep learning constructs hierarchical architectures of increasing sophistication, and deep learning neural networks with many perceived layers are examples of deep learning algorithms (Reichstein et al., 2019). Deep learning algorithms are now increasingly used to understand and model complex earth science problems and processes. Because it offers significant breakthroughs in solving classification and nonlinear regression problems (Sze et al., 2017) and can extract the valid features of data input through complex computational models and represent them at a higher level of abstraction, it eventually achieves complex self-learning functions through multiple transformations and combinations (LeCun et al., 2015). Traditional evaluation and analysis methods are often insufficiently effective in describing the continuous and quantitative rules in a complicated ecosystem (Moore et al., 2017), while deep learning may be an effective tool for dealing with this problem. In 2017, Lundberg and Lee (2017) proposed the SHapley Additive explained framework, based on the idea of sampling, to obtain the explainable process of complex predictive models, which can assign a contribution value for each input factor to the outcome of the association prediction; later, the framework was widely used in other fields (Lee et al., 2018; Wang et al., 2021). Liu et al. (2020a) established a deep learning neural network to approximate the ecosystem services (ESs) of Nanjing in China using 23 socioeconomic factors with good simulation performance. They disassembled the model based on sampling and found that the ecological water area and secondary industry were two key factors affecting ESs, while 23 independent and continuous driving relationship functions were obtained, proving the feasibility and advantages of applying deep learning in the exploration of the ecological driving mechanism.

After more than thirty years of rapid urbanization and industrialization, the Yangtze River Delta urban agglomeration (YRDUA) has developed into the sixth largest urban agglomeration in the world and the most economically developed region in China. At the same time, the regional ecological carrying capacity has also undergone profound changes with the continuous consumption of resources and energy during the past 20 years (Zhen et al., 2017). Previous studies have shown that rapid economic development in the YRDUA has consumed a large number of biological resources and energy, resulting in a gradual increase in EF, and the YRDUA is now the most unsustainable development region in China (Danish and wang, 2019; Yang et al., 2022). At the same time, there are numerous differences in ecological carrying capacity, urban resilience, urban scale, and industrial structure among the cities of the YRDUA. However, it is not clear how these differentials are intrinsically related to the differences in ecological carrying capacity evolution among regions, which makes it difficult to develop differentiated regional sustainable development regulation countermeasures.

Therefore, to better explore how human activities drive the regional ecological carrying capacity, we first assessed the ecological carrying capacity supply and demand balance index (ECCI) of the YRDUA cities from 2000 to 2019 based on a 3D EF model. Taking 2015, the year with the most dramatic regional socioeconomic changes, as an example, an artificial neural network model was constructed for each city based on deep learning algorithms to predict the regional ECCI using socioeconomic factors. Then, through model decomposition, independent driving effect curves were obtained, and the inner socioeconomic driving mechanism of the ECC evolution of each city was analyzed. Finally, the regional cities were classified according to the extracted urban ecological driving characteristics, which provided a more targeted decision basis for urban ecological construction and restoration in the YRDUA.

2. Materials and methods

2.1. Study area

Located on the eastern coast of China, the YRDUA is one of the most highly populated and developed regions of China (Wu et al., 2017). According to the “Outline of the integrated regional development of the Yangtze River Delta” issued in 2019, the YRDUA comprises the municipality of Shanghai, Jiangsu Province (JS), Zhejiang Province (ZJ), and Anhui Province (AH), which contains 41 cities in total. There is a huge development gap within the YRDUA, including megacities, large cities, and medium-sized cities, and there are huge differences in population density, economic development level, industrial structure, and even human activity intensity among cities and regions; for example, the level of economic development of AH is relatively backward, and the population density is relatively lower compared to JS and ZJ.

Therefore, given the urgent conflicts between land demand and limited land resources, the necessity of ecological restoration, and the complexity of regional heterogeneity, in this study, we chose the YRDUA as the study area. Considering the requirements of the data sample size for deep learning training, the area of the target city should be large enough to be assigned to hundreds of samples for model training and testing. Because the area of Zhoushan city in ZJ, which is directly relevant to the sample size, is too small, and it includes a lot of tiny pieces of islands that cannot be extracted as samples for model training or testing. As a result, Zhoushan was excluded from the study area. Hence, as shown in Fig. 1, there are finally 40 cities contained in our study area, including Shanghai city, 13 cities in JS, 10 cities in ZJ, and 16 cities in AH.

2.2. Dataset

As the past decade was the most rapidly developed period of the YRDUA, taking the data accessibility into account as well, we

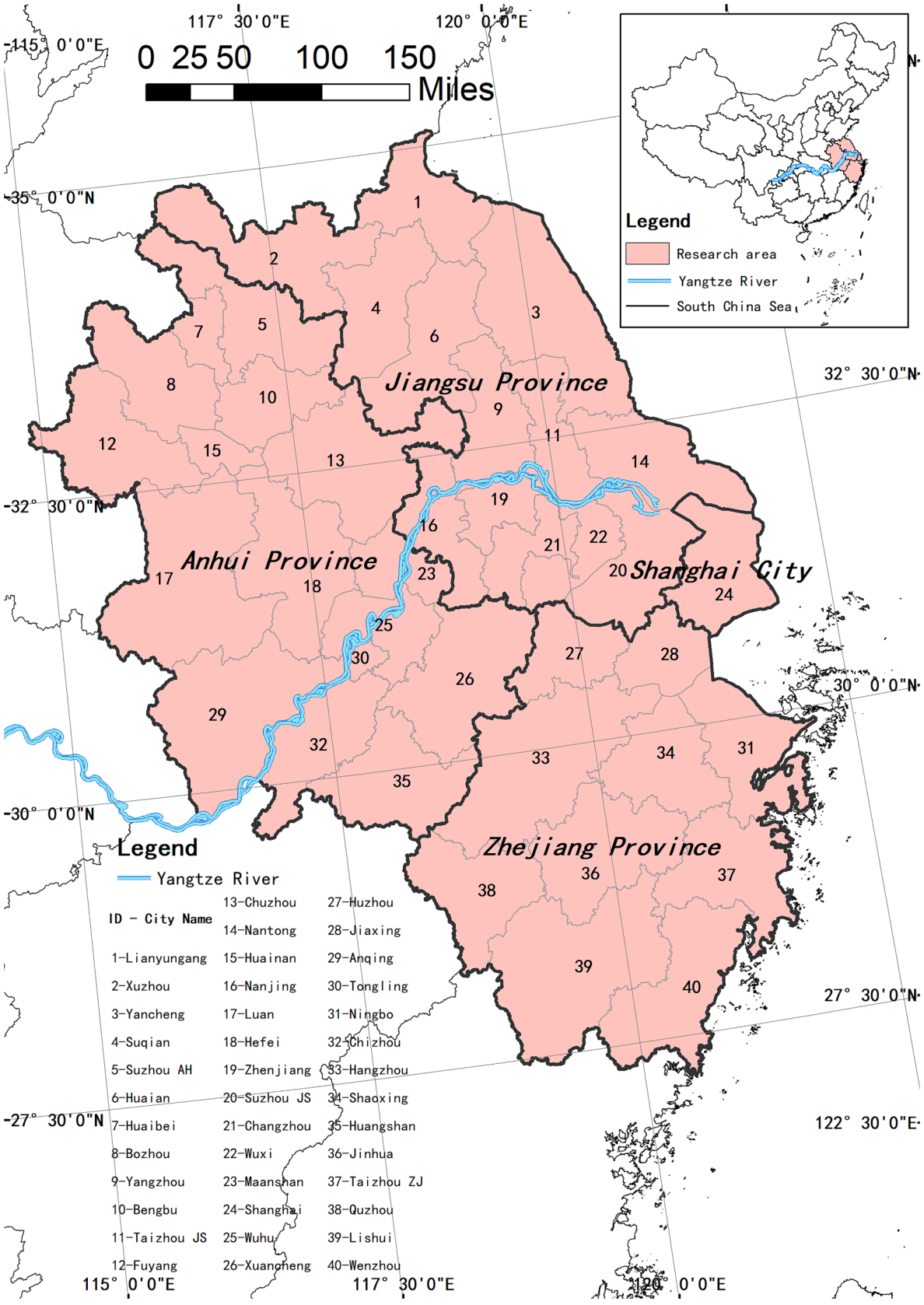

Fig. 1. Map of the YRDUA.

constructed the YRDUA socioeconomic-ecological dataset from 2000 to 2019 for estimating ecological sustainability and modeling the spatial socioeconomic-ecological relationships. The data used in this study included 4 aspects, socioeconomic, agricultural, energy consumption, and land use data. Because agricultural consumption data are difficult to obtain, we used agricultural production data as an alternative. Both agricultural production data and energy consumption data were obtained from the Statistical Yearbooks of cities in the YRDUA for 2001, 2006, 2011, 2016, and 2020. The accounting factors as inputs for EF models are shown in Table 1.

The land use data were derived from the National Tibetan Plateau Data Center (https://data.tpdc.ac.cn/zh-hans/). The dataset has a resolution of 1 km*1 km based on Landsat 8 remote sensing images and is generated by visual interpretation. It includes 6 primary types, i.e., cropland, woodland, grassland, water, residential land, and unused land, and 25 secondary types.

According to the availability of data, whether it can be spatialized, the correlation with ECC, and whether it was used to estimate ECC and EF, 11 socioeconomic factors were selected as the input factors of the deep learning model, including gross domestic product (GDP), population density, light intensity, light area, NDVI index, road network density, scenic spot density, carbon dioxide emissions, and output value of the primary, secondary, and tertiary industries (Table A1) (hereafter shown as OV1, OV2, OV3). Among them, although the NDVI index is often used as a natural ecological indicator reflecting vegetation cover, it was also introduced as a socioeconomic indicator reflecting the intensity of land use in the process of urban development, which conversely indicates the encroachment or restoration of green space. Road network density was collected as an indicator of urban construction. Scenic spot density was collected as an indicator of tourism development and ecological management. Carbon emissions were collected as an indicator of energy consumption. The industry output value data were collected from the statistical yearbook, which was nonspatial data and needed to be spatialized for modeling input data format requirements. Due to the construction of the YRDUA ECC prediction model in 2015, socioeconomic data were updated in 2015 as well, except for the light index in 2013.

2.3. Methods

2.3.1. Ecological footprint model

The EF model was introduced into this study to estimate the ECC of the study area at the city level, which was the output of the deep learning model (Fig. 2). The EF model includes EF estimation, BC estimation, and the calculation of the ECCI. The ECCI was introduced to measure the regional carrying capacity condition which was set as the output of the deep learning models. According to the EF models improved by Hong (Hong et al., 2020; Wackernagel et al., 1999a,b), the total EF consists of the biological ecological footprint (BEF), energy ecological footprint (EEF), and pollution ecological footprint (PEF) (in Eq. (1). A total of 27 factors were selected for the ecological footprint account (Table 1) and based on the EF account and Eqs. (2)–(4), the BEF, EEF, and PEF could be calculated.

Table 1
EF accounting factors.

Production land use type	Accounting factors
Cropland	Rice, wheat, corn, beans, potatoes, cotton, oilseeds, vegetables
Grassland	Pork, lamb, beef, milk, poultry eggs, poultry meat
Woodland	Fruits, timber
Water	Aquatic products
Construction land	Electric energy
Fossil fuel land	Coal, gasoline, kerosene, diesel, fuel oil, natural gas
Pollution consumption land	Industrial wastewater, SO_2 emissions, solid waste

$$EF = BEF + EEF + PEF \tag{1}$$

$$BEF = \sum_{j=1}^{5}\left[r_j \times \sum_{i=1}^{n} c_i/\overline{p_i}\right] \tag{2}$$

where BEF is the total EF of bioresource consumption in arable land, woodland, grassland, water area, and urban construction land, j is the bio-productive land-use types, r_j is the equivalence factor of land use j, i is the accounting factor (i.e., bioresource category in the calculation of BEF), c_i is the total amount of bioresource i, and p_i is the average production of bioresource i in China.

$$EEF = n_i{*}ec/ep \tag{3}$$

The calculation of EEF is according to the concept of a "carbon sink". where n_i is the total amount of accounting energy type I, ec is the emission coefficient, and ep is the average carbon absorption capacity of bio-productive land. The ec values of coal, gasoline, kerosene, diesel, and fuel oil are 0.57, 0.85, 0.88, 0.87, and 0.85, respectively. The ec of natural gas is 0.00047 t/m^3, while ep is 4.45 hm^2/t (Chen et al., 2020b; Yang and Fan, 2019).

Industrial wastewater, SO_2 emissions, and solid waste were taken into account when calculating the ecological pollution footprint in equation (4) (Bai et al., 2008).

$$PEF = \sum u_i/e_i \tag{4}$$

where u_i is the total amount of accounting pollution type i and e_i is the decontamination factor of pollution type i. The average consumption of industrial wastewater per unit of water area in China is 365 t/hm^2, the adsorption capacity of SO_2 per unit of forestland is 152.05 kg/hm^2, and the amount of solid waste that can be accumulated per unit area of land is 109000 t/hm^2.

BC could be calculated according to land use as shown in equation (5):

$$BC = \sum_{j=1}^{n}(a_j \times r_j \times y_j) \tag{5}$$

where a_j is the area of land use type j, r_j is the equivalence of land use type j, y_j is the yield factor of land use type j, and n is the number of land-use types, which is 6 in this study. According to the report "Out common future" (Butlin, 1989), 12% of the total bioproductive area was deducted as biodiversity conservation. The equivalence factors and field factors of the YRDUA are shown in Tables A2 and A3 (Hong et al., 2020; Liu et al., 2015).

Finally, the ECCI was calculated according to equation (6). When ECCI < 1, the supply of the ecosystem is more than the demand, and there is an Ecological Remainder or Credit; when ECCI > 1, the demand of the ecosystem is more than the supply, and there is an Ecological Overshoot or Deficit, which means the demand for natural resources exceeds the regenerative capacity of existing natural capital. The ECCI was calculated using equation (6). According to the definition and understanding of ECCI, the YRDUA could be divided into three categories, as shown in Table A4 (i.e., ecological surplus region, ecological demand–supply balanced region, and ecological deficit region) based on the evaluation criteria (Liu et al., 2011), and 13.87 is the mean ECCI of YRDUA.

$$ECCI = EF/BC \tag{6}$$

2.3.2. Data preprocessing and spatialization

Multidata fusion on the same scale is necessary to ensure that the labeled samples meet the common format and quantity requirements for deep learning model training (Hodgkinson and Andresen, 2019). Because the ECCI is influenced by a multiplicity of socioeconomic and natural factors, if the selected spatial unit is too small, then demonstrating the composite effect will be difficult. Moreover, model training

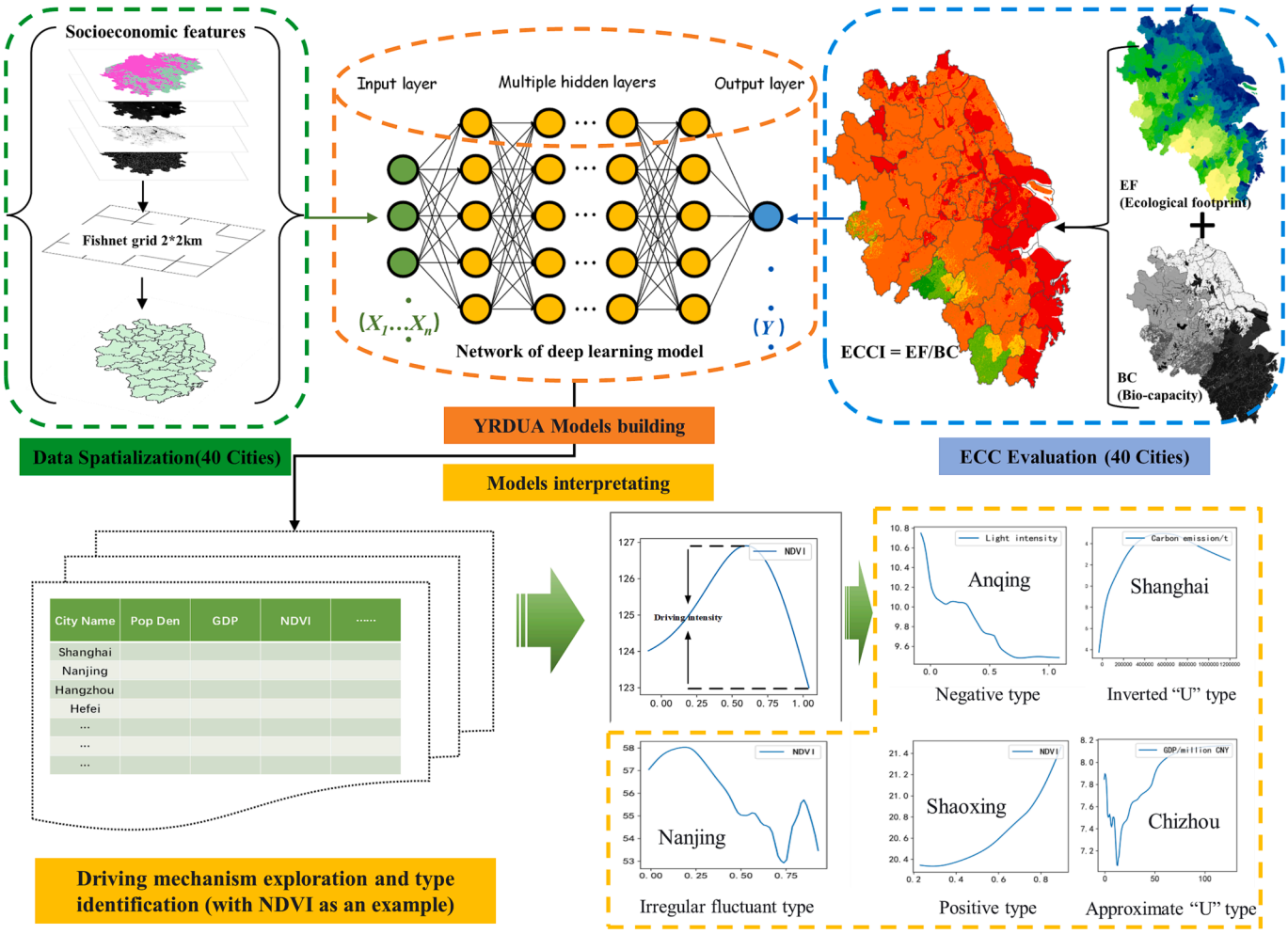

Fig. 2. The flowchart of model construction and analysis.

and testing have a minimum requirement for the sample size. Therefore, we used a 2 km*2 km grid, which is better than the 1 km*1 km and 5 km*5 km grids, for data processing by grid transformation. The spatial data (i.e., GDP, population density, NDVI index, carbon emissions, etc.) was downscaled to 2 km*2 km using zonal statistics in ArcGIS (Fig. 2), and the sample size of each model is the pixel numbers in each city (Table A5).

Light intensity and light area were calculated based on the DMSP/OLS nighttime light data, as shown in Eqs. (7) and (8).

$$I = I^{'}/(A \times DN_{\max}) \tag{7}$$

$$S = S^{'}/A \tag{8}$$

where I is the light intensity, I' is the sum of the DN values within a unit, A is the area of a unit, DN_{max} is the maximum DN value, which is 63, S is the light area proportion, and S' is the area within a unit where the DN value is not 0.

Scenic spot density was calculated based on the scenic spot list. Google Geocoder and Map location were used to obtain location data that could be imported into ArcMap for spatial analysis. The scenic spot density map was obtained by spatial interpolation using the Kriging approximate grid algorithm in ArcGIS.

Road network density was calculated based on highway network data. Spatial overlay analysis tools were used to cut, identify, and summarize the highway length in each grid, and then the road network density was the quotient of highway length and the area of the grid.

OV1, OV2, and OV3 are statistical data that need to be spatialized to meet the requirements of the input data. OV1 is closed relative to land-use type; therefore, the sum of OV1 was assigned by land-use proportion (Eq. (9) (Zongguang et al., 2016). The primary industry consists of agriculture, forestry, livestock husbandry, and fishery, which correspond to cropland, woodland, grassland, and water area, respectively.

$$G_1 = \sum_{j=1}^{4} G_{ij} \times (a_j/A_{ij}) \times P_{ij} \tag{9}$$

where G_1 is OV1 within a unit and G_{ij} is the output value of the sector j of OV1 in the city i. OV1 consists of agricultural (j = 1), forestry (j = 2), livestock husbandry (j = 3), and fishery (j = 4). a_j is the area of productive land of the corresponding OV1 sector within a unit, i.e. cropland (j = 1), woodland (j = 2), grassland (j = 3), water (j = 4). A_{ij} (j = 1, 2, 3, and 4) is the sum of the areas of cropland, woodland, grassland, and water, respectively, in city i. P_{ij} (j = 1, 2, 3, and 4) is the proportion of agricultural, forestry, livestock husbandry, and fishery, respectively in OV1 of city i.

OV2 and the tertiary industry were spatialized based on the nighttime light imagery(Han et al., 2012), and the fitting accuracy of the regression model in YUDRA was high, where R^2 was over 0.7, as shown below (Eqs (10) and (11):

$$GDP_i = e^p \times I^a \tag{10}$$

$$GDP_i^{'} = GDP_i \times (GDP_{isum}/GDP_{iall}) \tag{11}$$

where GDP_i is OV2 or OV3 of city i, p, and a are coefficients for fitting models, where p = 14.424, a = 0.733 for OV2, and p = 13.795, a = 0.58

for OV3, i is the light intensity of the unit, GDP_i' is OV2/OV3 in the unit of city i after correction, GDP_{isum} is the sum of the unit OV2/OV3 of city i, and GDP_{iall} is the statistical OV2/OV3 of city i.

The spatialization of ECCI was based on the assumption that the EF per capita in the same region was similar. Therefore, EF was assigned by population density as shown in Eq. (12), and ECCI could be obtained by calculating the quotient of spatial EF and BC. Because of the absence of population density data in 2019, only the ECCIs in 2000, 2005, 2010, and 2015 were spatialized.

$$Ef_j = EF_i / P_i \times p_j \tag{12}$$

where Ef_j is the EF in unit j, EF_i is the sum of EF in city i, P_i is the population in city i, and p_j is the population in unit j.

2.3.3. Deep learning model construction:

Because of the complexity of the anthropogenic driving mechanisms, the more essential and quantifiable relationships of the independent socioeconomic variables for ECCI are difficult to describe with conventional models (Ahmed et al., 2021; Wang and Dong, 2019). We chose multilayer perception as the deep learning model, which is also called the multilayer feedforward dense network. It is a generic nonlinear function approximation algorithm that has been extensively used for problems such as function approximation, prediction, and classification. It is the most widely used type of network because of its flexibility and simple structure, which are also beneficial to the subsequent model analysis. In this study, independent models were constructed in 40 cities with different structures. Various models for each city were established with different parameters and compared to determine the best models with the highest explanatory power and predictive power for 40 cities. All the models consist of at least 8 layers (4 dense layers), including an input layer (11 socioeconomic facots), an output layer (ECCI), and at least 6 hidden layers (Table 2), but with different numbers of uncertain layers, active functions of uncertain layers, and numbers of neurons (Table A5) (Qi et al., 2020; Wang et al., 2021; Wang et al., 2020b). Taking Nanjing as an example, the number of uncertain layers is 2, and the active functions are both tanh, so there are two dense layers (in a total of 4 dense layers) with tanh as the active functions and two dropout layers. The neuron numbers are 1024, 128, 64, and 16, so the four dense layers have 1024, 128, 64, and 16 neurons, respectively. Nonlinear activation functions, such as the rectified linear unit and tanh, were introduced in hidden layers to learn the nonlinearity and avoid vanishing gradient problems. The linear active function was introduced to the first and the last dense layers to linearly combine all the former parameters, which was conducive to model disassembly and interpretation. Additionally, the dropout rate was set to 0.3 in all dropout layers to avoid overfitting problems (Wang et al., 2020a).

The construction and training of the deep learning neural network were conducted in Python 3.6.8 with Keras, which is a deep learning API running on top of the machine learning platform TensorFlow. We partitioned 70% of the unit samples of every city as training samples and 30% as testing samples. Data standardization was conducted before training to eliminate the influence of the magnitudes. In the training phase, the optimizer and loss function were established based on the adaptive moment estimation (ADAM) and mean square error (MSE) (Eq. (13)). After conventional model optimizations were performed, the above hyperparameters were determined. The corresponding model was trained and used in the study. The model assessment was based on the Nash-Sutcliffe efficiency (NSE) and RMSE (Root mean square error)-observations standard deviation ratio (RSR), which contributed to the parameter regulation and model optimization as well (Eqs (14)–(16)).

$$MSE = \sum_{i=1}^{n} \left(Y_i^{obs} - Y_i^{sim}\right)^2 / n \tag{13}$$

$$NSE = 1 - \left[\sum_{i=1}^{n} \left(Y_i^{obs} - Y_i^{sim}\right)^2 / \sum_{i=1}^{n} \left(Y_i^{obs} - Y^{mean}\right)^2 \right] \tag{14}$$

$$RMSE = \sqrt{\sum_{i=1}^{n} \left(Y_i^{obs} - Y_i^{sim}\right)^2 / n} \tag{15}$$

$$RSR = RMSE / STDEV_{obs} = \left[\sqrt{\sum_{i=1}^{n} \left(Y_i^{obs} - Y_i^{sim}\right)^2} \right] \Big/ \left[\sqrt{\sum_{i=1}^{n} \left(Y_i^{obs} - Y^{mean}\right)^2} \right] \tag{16}$$

where Y_i^{obs} is the observation of the i^{th} sample, Y_i^{sim} is the simulation of the i^{th} sample, Y^{mean} is the mean of the observations, and n is the sample size.

2.3.4. Analysis and classification of ecological carrying capacity driving methods for different cities

Simply making predictions, without explanation, are in most cases unconvincing and provides little insight into how we should respond to changing EF and BC. In this context, the interpretation of deep learning learning neural networks required a deeper dive into the data for interpreting feature impact that provided insights into how the output was determined or improved (Wang et al., 2021). SHapley Additive exPlanations is a game-theoretic approach to explain the output of any machine learning model based on the sampling idea applied to every feature and every sample (Stojić et al., 2019). According to this approach, we observed how ECCI (Y) responded to the change in each feature (X) by sampling continuously in the range of each input X. In the course of the concrete analysis, other features were kept as the mean of the samples, and the values of the target features were changed by adopting control variables. Additionally, the range of the target feature was regarded as its definition domain, called the sampling domain. The ECCI range varies in terms of the target X in its sampling domain, which is called the response domain. The driving intensity of every feature can be judged according to the corresponding response domain (Fig. 2), and the potential mechanism can be judged according to the variation trend of the driving effect curves (Fig. 2).

After feature explanation, the contribution (driving intensity) of 11 features was extracted to describe the ecological driving patterns of cities. The most important information of 11 features was extracted and simplified by principal component analysis (PCA) (Abdi and Williams, 2010). According to the principal components, 40 cities could be classified into different types based on k-means cluster analysis. After merging and reclassifying, final types of cities with different significant features could be interpreted and understood.

Table 2
The main structure and parameters of the 40 models.

	Hidden layers	Parameters	
		Active function	Numbers of neurons
Input layer	dense	/	11 (socioeconomic factors)
The first two-hidden layers	dense dropout	linear 0.3	n
Uncertain layers	dense dropout	tanh or elu 0.3	n
The last two-hidden layers	dense dropout	ReLU 0.3	n
Output layer	dense	linear	1 (ECCI)

3. Results

3.1. Model accuracy

The accuracy of the 40 models was classified into 4 levels (Tables A6 and A7) based on the evaluation criteria of NSE and RSR (Table A6). At

the province scale, the average model accuracy of JS and ZJ both reach the "Very good" level (NSE > 0.75, RSR ≤ 0.5), while the average NSE of the models in AH is 0.73. At the city scale, all 39 models except the Tongling model (NSE = 0.286, RSR = 0.845) reach the "Satisfactory" level or above. 32 out of 40 models are "Very good", and the highest NSE (0.97) and lowest RSR (0.173) both belong to the Shanghai model. 5 out of the 40 models are "Good", 2 out of the 40 models are "Satisfactory", and 1 model is "Unsatisfactory" (Tongling city), which means that this model cannot be trusted, and the model of Tongling city was excluded in the following sections. In other words, the dominant socioeconomic divers and driving mechanism of 39 cities will be analyzed and interpreted.

3.2. Identification of important drivers

According to the response domain (Fig. 2), the driving intensity (DI) of 11 socioeconomic features were defined and extracted from 39 valid prediction models. As shown in the box plot (Fig. 3), "Population density" exerts the most important impact on ECCI, with the highest value and low variation of DI. In addition, the median DI value of "Population density" is nearly 0.8. While "road network density" and "scenic spot density" both have a low value of DI, indicating a nonsignificant impact on ECCI, the median values are both less than 0.2. It can also be observed that the DI values of "GDP", "OV1", "OV2", and "OV3" ("output value of the primary, secondary, and tertiary industries") are also relatively important, with median values are all more than 0.3.

At the city scale, there is significant variation among the DI of different cities in the same feature. To better illustrate the results, the DI value was divided into three levels: "High" (DI ≥ 0.5), "Medium" (0.3 ≤ DI < 0.5), and "Low" (DI ≤ 0.3). The driving intensity level of "Population density" in Huangshan is "Medium", but it in the other 38 cities is "High", which demonstrates that the ECCI of most of the cities in YRDUA is mainly driven by "Population density" (Table 3). Shanghai has the highest DI value, which is 0.94. For "GDP", the level of driving intensity of 10 cities is "High". Among them, Huaibei, Bengbu, and Huzhou have medium DI values of 0.78, 0.76, and 0.7, respectively (Table 3). In addition, 13 cities have a "Medium" level driving intensity of "GDP", and 16 cities have a "Low" level. Huaian is the only city that has the "High" level of driving intention of "Light intensity" or "Light area proportion". In contrast, the driving intensity levels of "light intensity" and "light area proportion" of most cities are "Low" (31 and 35) (Table 3). Four cities have high DI values of "NDVI", but the they are all just over 0.5. The driving intensity of "carbon emissions" of five cities is "High"; among them, Nantong has the highest DI value, which is 0.71, demonstrating that ECCI in Nantong is strongly driven by "carbon emissions". For industrial structure, the numbers of cities with "High" driving intensity levels of "OV2" and "OV3" are more than "OV1", which are 15, 14, and 8, respectively. The ECCIs in Chuzhou (0.67) and Quzhou (0.65) are strongly driven by "OV1", the ECCIs in Huaibei (0.84) and Wuhu (0.81) are strongly driven by "OV2", and the ECCIs in Wuhu (0.83) and Xuzhou (0.82) are strongly driven by "OV3" (Table 3). No city has the "High" level of driving intensity of "Road network density" and "Scenic spots density"; ECCI is driven by "Scenic spots density" with high driving intensity in only 5 cities. In contrast, the ECCI is driven by the two features with low driving intensity in other cities (Table 3).

3.3. Driving effect curves of different features

According to the shape of the relationships between the ECCI and 11 socioeconomic features of 39 cities in the YRDUA, 5 types of driving effect curves could be obtained, i.e., positive, negative, "U"-shaped, inverted "U"-shaped, and irregularly fluctuant. As shown in Table 4, the dominant driving effect curves of the 11 features are different. The driving effect curve between "Population density" and ECCI in 37 out of 39 cities are all positive, while those in Yangzhou and Hefei are "U" shaped, demonstrating that ECCI in most of the cities in YRDUA will

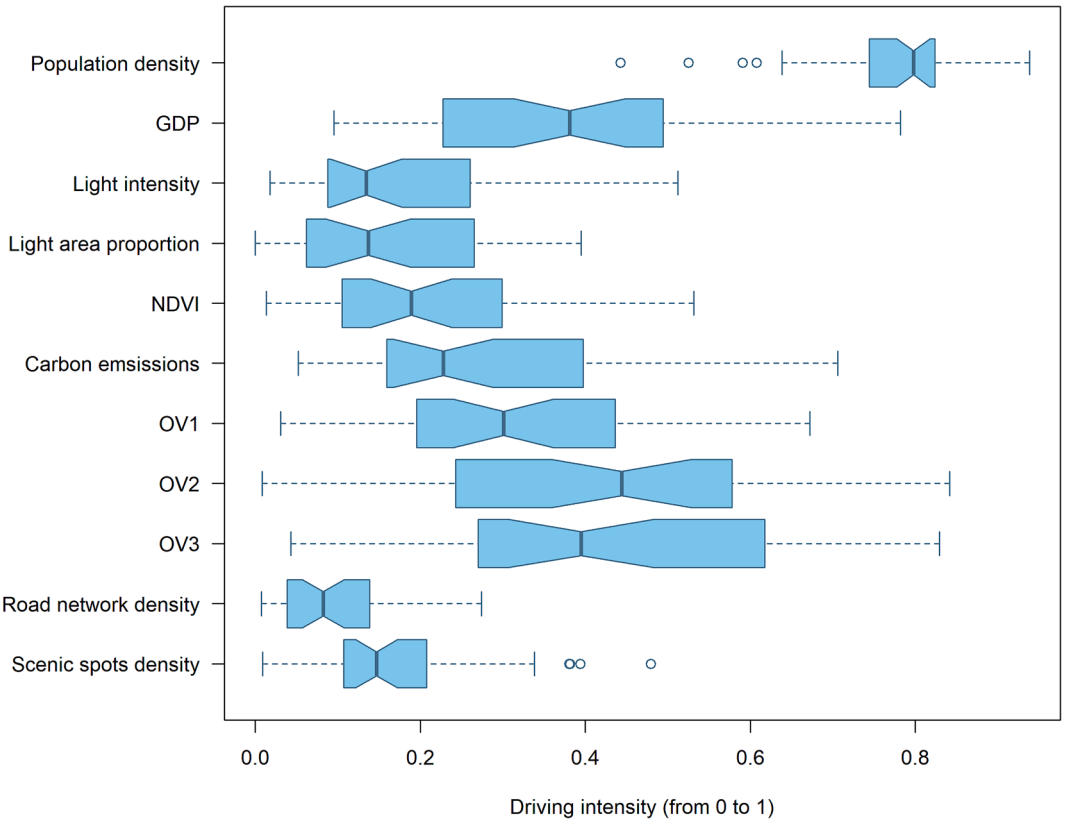

Fig. 3. Box plot of the driving intensity of 11 features in 39 cities.

Table 3
The driving intensity of the 11 features of cities in the YRDUA.

	High level of driving intensity		Medium level of driving intensity		Low level of driving intensity
Feature names	Numbers	Example cities	Numbers	Example cities	Numbers
Population density	38	**Shanghai (0.94),** Nanjing, Hefei, Hangzhou	1	Huangshan	0
GDP	10	**Huaibei (0.78), Bengbu (0.76), Huzhou (0.7)**	13	Changzhou, Hefei, Anqing, Shaoxing	16
Light intensity	1	**Huaian (0.51)**	7	Yangzhou, Huaibei, Luan, Jinhua	31
Light area proportion	0	/	4	Suzhou JS, Changzhou, Taizhou JS, Huaian	35
NDVI	4	Yangzhou (0.53), Huaian (0.53), Suqian (0.5), Luan (0.52)	6	Changzhou, Taizhou JS, Anqing, Huangshan, Xuancheng, Chizhou	29
Carbon emissions	5	**Nantong (0.71),** Xuzhou, Anqing, Chizhou, Hangzhou	9	Suzhou AH, Suqian, Wenzhou, Huzhou	25
OV1	8	**Chuzhou (0.67), Quzhou (0.65),** Wuxi, Anqing	12	Nanjing, Zhenjiang, Yancheng, Maanshan	19
OV2	15	**Hauibei (0.84), Wuhu (0.81),** Xuzhou, Suqian, Fuyang	12	Jinhua, Luan, Chizhou, Xuancheng	12
OV3	14	**Wuhu (0.83), Xuzhou (0.82),** bozhou, Hefei	14	Huainan, Lianyungang, Shaoxing	11
Road network density	0	/	0	/	39
Scenic spots density	0	/	5	Suzhou, Wuxi, Changzhou, Xuancheng, Chuzhou	34

"/" means no data, and the relatively high value is in bold font.

increase with population growth. The dominant driving effect curve of "GDP" is also positive, illustrating that ECCI will increase with economic development. In addition, there are also 12 out of 39 cities, such as Hangzhou and Suzhou JS, where the ECCI will show a trend of rising first and then falling with the increase in "GDP", indicating greener and more sustainable economic development.

OV1, OV2, and OV3 are also important features with high DI values. The driving effect curves of OV1 and OV3 were both negative, while those of OV2 were positive. It could be concluded that OV1 and OV3 in the YRDUA are more sustainable than OV2, leading to a possible ECCI decrease with continuous economic development, while OV2 will bring more environmental pressure under the same economic benefits that need to be controlled. In addition, there are also inverted "U"-shaped driving effect curves of OV1, OV2, and OV3 in 9, 6, and 6 cities, respectively, which means that there is a threshold of industry development, and the ECCI will decrease after crossing the threshold. However, the threshold values of the inverted "U"-shaped driving effect curve and "U"-shaped driving effect curve of different cities and different features are different, which has not been shown in this study. For regional ecological protection and restoration, a more specific and quantitative analysis of the driving effect curve of the target socioeconomic sector should be conducted.

Empirically, the urbanization process would lead to an increase in ECCI. However, the main driving effect curves of "Light intensity" and "Light area proportion" are both negative, which means that ECCI will decrease, indicating some degree of ecological restoration with the rapid urbanization process. In addition, 12 and 19 cities have positive or inverted "U"-shaped driving effect curves of "light intensity" and "light area proportion", respectively, which meets the understanding of the relationship between ECC and urbanization in previous research.

The main driving effect curve of the NDVI is negative, which demonstrates that the protection of vegetation, especially in an urban area, could benefit the falling of the ECCI. There are two main driving effect curves of "carbon emissions", which are positive and inverted "U" shaped, in 15 and 14 cities, respectively. "Carbon emission" is the indicator of energy consumption of a region, and the ECCI of a region will rise with the increase in energy consumption. However, in 14 cities, such as Shanghai and Hangzhou, there is a threshold at which the ECCI will decrease when the carbon emissions exceed it, which may be caused by a cleaner energy structure or technological advancements.

3.4. Identification and classification of the dominant drivers of ECC in different cities

After ordination analysis using PCA, 6 principal components (PCs) were obtained with an 87.26% cumulative explained variance ratio (Table A8). First, according to the variable loadings, 6 PCs could be interpreted (Table A9). The absolute values of the "OV1", "OV2", and "OV3" loadings of PC1 are higher and are negative at the same time. Therefore, PC1 includes information about the industrial structure, and the smaller PC1 is, the more strongly the ECCI is driven by the industrial structure. By the same logic, PC2 mainly includes information about "Light intensity", "NDVI", "OV1", and negative "OV3", which are all related to the land urbanization process. PC3 mainly includes information about positive GDP and negative carbon emissions, and the larger PC3 is, the more strongly the ECCI is driven by GDP. In contrast, the small PC3 score demonstrates that the ECCI is more likely driven by "carbon emissions". PC4 mainly includes information about the industrial structure and carbon emissions, and OV1 and OV3 are positive, while OV2 and carbon emissions are negative. PC5 mainly includes information about "Population density" and "Light intensity", which are related to population urbanization. PC6 mainly includes information about positive "carbon emissions", "GDP", and "OV2", which are relative to energy consumption.

Then, the 39 cities in the YRDUA were classified into 4 clusters using the K-means cluster method based on the 6 PC scores (Table 5). According to the mean PC scores, each type could be analyzed and named different types of ECC driving patterns. Type 1 includes 11 cities, such as Suzhou JS, Wuxi, and Changzhou, and the PC2 score is high, indicating that this type is mainly driven by "Light intensity", "NDVI", or "OV1", which are all related to the land urbanization process. Therefore, type 1 cities were named urban expansion driving. Type 2 includes 13 cities, such as Nanjing and Hefei, which have the highest score of PC3, which illustrates that the DI of "GDP" is high, while that of "carbon emissions" is low. Therefore, the ECC driving patterns for type 2 cities could be summarized as green economy driving, which means that regional ECCI regulation relies on finding a rational green economic development pattern. Type 3 includes 7 cities, such as Xuzhou and Anqing. The score of PC1 is the lowest among the 4 types of cities, indicating that the DIs of "OV1", "OV2", and "OV3" are high. The PC3 score of type 3 is also the lowest, indicating a high DI of "carbon emissions". In addition, type 3 cities also have the highest PC4 score, which means high DI of "OV1" and "OV3" or low DI of "OV2" and "Carbon emissions". All these

Table 4
The classification of driving effect curves of 11 socioeconomic features.

Feature names	Driving effect curves	Counts	Examples
Population density	**Positive**	**37**	**Shanghai, Nanjing**
	"U"-shaped	2	Yangzhou, Hefei
GDP	**Positive**	**20**	**Anqing, Changzhou**
	Negative	3	Shanghai, Hefei
	"U"-shaped	3	Chizhou, Suzhou JS
	Inverted "U"-shaped	12	Hangzhou, Shaoxing
Light intensity	Positive	3	Shanghai, Wenzhou
	Negative	**19**	**Anqing, Xuancheng**
	"U"-shaped	3	Taizhou, Suqian
	Inverted "U"-shaped	9	Hangzhou, Suzhou JS
	Irregularly fluctuant	3	Maanshan, Chizhou
Light area proportion	Positive	11	Nanjing, Huzhou
	Negative	**14**	**Taizhou, Wenzhou**
	"U"-shaped	5	Wuxi, Wuhu
	Inverted "U"-shaped	8	Xuzhou, Ningbo
NDVI	Positive	7	Shaoxing, Wenzhou
	Negative	**15**	**Suzhou JS, Suqian**
	"U"-shaped	5	Wuxi, Jinhua
	Inverted "U"-shaped	10	Shanghai, Wuhu
	Irregularly fluctuant	2	Nanjing, Quzhou
Carbon emissions	**Positive**	**15**	**Jinhua, Shaoxing**
	Negative	8	Xuzhou, Suzhou
	"U"-shaped	2	Suzhou JS, Wuxi
	Inverted "U"-shaped	**14**	**Shanghai, Hangzhou**
OV1	Positive	1	Huaibei
	Negative	**21**	**Nanjing, Yangzhou**
	"U"-shaped	7	Suqian, Wenzhou
	Inverted "U"-shaped	9	Shanghai, Yancheng
	Irregularly fluctuant	1	Taizhou
OV2	**Positive**	**18**	**Nanjing, Yangzhou**
	Negative	13	Xuzhou, Taizhou
	"U"-shaped	2	Huzhou, Nantong
	Inverted "U"-shaped	6	Shanghai, Yancheng
OV3	Positive	10	Lishui, Jiaxing
	Negative	**21**	**Nanjing, Yancheng**
	"U"-shaped	2	Taizhou, Suzhou JS
	Inverted "U"-shaped	6	Shanghai, Yangzhou
Road network density	Positive	8	Shanghai, Anqing
	Negative	**14**	**Nanjing, Wuxi**
	"U"-shaped	6	Huzhou, Wenzhou
	Inverted "U"-shaped	10	Jiaxing, Ningbo
	Irregularly fluctuant	1	Luan
Scenic spots density	Positive	10	Nanjing, Suzhou JS
	Negative	4	Huaibei, Yangzhou
	"U"-shaped	6	Shaoxing, Anqing
	Inverted "U"-shaped	**16**	**Shanghai, Wuhu**
	Irregularly fluctuant	3	Suqian, Huaian

The dominant driving effect curve type is in bold font.

features are relevant to industrial structure and energy consumption. Hence, type 3 cities could be named ecological industrial structure driving patterns. Finally, type 4 includes 8 cities, such as Shanghai and Hangzhou, where the scores of PC1 and PC5 are high. A high DI of "Population density" will lead to a high PC1 score, and a high PC5 score also means a high DI of "Population density" and "Light intensity". Therefore, the ecological urban driving patterns of type 4 cities could be named population density driving. For example, there is only "Population density" one feature with "High" level driving intensity(DI $>$ 0.5) of Shanghai and Jiaxing, while the other 10 features are all "Low" level driving intensity (DI $<$ 0.3).

3.5. The spatial distribution and temporal changes of ECCI in the YRDAU

As shown in the bar graph of ECCI at the province scale and the city scale (Fig. A1), three provinces and most of the cities all showed an increasing trend of ECCI first and then showed a decreasing trend. However, the ECCI value of 2019 was still obviously higher than that of 2000 in most of the cities and provinces. To better infer and discuss the urban ECC driving mechanism and patterns, the ECCI spatial distribution from 2000 to 2015 was mapped and analyzed (Fig. 4). According to the ECCI value, the condition of ecological demand–supply balance was divided into 6 levels (Table A4), and most of the regions in YRDAU were still in the "Obvious overloading" level and the "Serious overloading" level. The "Balance" region, "Surplus" region, and "Over surplus" region were only existed in Luan, Xuancheng, Anqing, Chizhou, Huangshan, and Lishui during the 15 years. In addition, there were "Balance" regions, "Surplus" regions, or "Over surplus" regions only in Luan, Huangshan, and Lishui. In contrast, the "Seriously overloading" area expanded during the 15 years, especially in the southeastern coastal region and cities around Shanghai. This ecological deterioration might be led by the increasing population density and unsustainable economic development.

4. Discussion

4.1. Significant diversity and spatial aggregation differentiation of urban ECC driving patterns in the YRDUA

According to the spatial visualization of urban ECC driving patterns, the spatial distribution of ecological driving mechanisms in the YRDUA could be analyzed and concluded (Fig. 5a). The first type of cities, i.e., urban expansion-driving, are only distributed in AH (5 cities) and JS (6 cities). In addition, these cities are distributed around Nanjing city, which might indicate the role of urban radiation in Nanjing to the south area of AH and the middle of JS. The second type of cities, i.e., green economy-driving, spread broadly across the three provinces but is mainly located in the middle of each province, such as Hefei, Zhenjiang, Jinhua, and Shaoxing. The third type of cities, i.e., industrial structure-driving, are distributed only in AH and JS, mainly in the northern area of the two provinces at the same time. The cities located in the north of AH and JS have similar industrial structures and resource-intensive pillar industries, forcing environmental pressure (Liu et al., 2021; Wang et al., 2013), which might explain why they were divided into industrial structure-driving. Finally, the fourth type of cities, i.e., population density-driving, are coastally distributed in JS and ZJ, including Shanghai. Among the 8 population density-driving cities, Yancheng, Nantong, Shanghai, Jiaxing, Ningbo, and Wenzhou are all coastal cities, accounting for 75%.

At the province scale, there are four types of ECC driving patterns distributed in JS with an agglomerate effect. Industrial structure-driving cities are located in the north of JS, urban expansion-driving cities are located in the middle and south of JS, Nanjing and Zhenjiang are green economy-driving types, and the coastal areas, including Yancheng and Nantong, are population density-driving type. Three types of ECC driving patterns were evenly distributed in Anhui without the population density-driving types. The 10 cities in ZJ could only be divided into the green economy-driving type and population density-driving type, and the north and south of ZJ are mainly the population density-driving type, while the green economy-driving cities are only distributed in the middle of ZJ except Huzhou, which is at the intersection of JS, AH, and ZJ.

In short, the ECC driving patterns of different cities in the YRDUA show significant diversity, spatial differentiation, and aggregation. It is likely that these characteristics have enabled so many cities to form

Table 5
The classification and nomination of ECC driving patterns in the YRDUA.

City Types	City Name	Counts	PC scores mean						ECC driving patterns
			1	2	3	4	5	6	
1	Suzhou JS, Wuxi, Changzhou, Taizhou JS, Yangzhou, Chizhou, Chuzhou, Huaian, Xuancheng, Maanshan, Luan	11	−0.13	**0.28**	−0.02	−0.04	−0.02	0.02	Urban expansion-driven
2	Nanjing, Lianyungang, Zhenjiang, Hefei, Huainan, Huaibei, Bengbu, Huangshan, Jinhua, Shaoxing, Taizhou ZJ, Quzhou, Huzhou	13	−0.01	−0.12	**0.18**	0.01	−0.01	0	Green economy-driven
3	Xuzhou, Suqian, Anqing, Wuhu, Fuyang, Suzou AH, Bozhou	7	**−0.30**	−0.19	**−0.18**	**0.07**	−0.01	−0.03	Industrial structure-driven
4	Shanghai, Hangzhou, Jiaxing, Ningbo, Wenzhou, Lishui, Yancheng, Nantong	8	**0.45**	−0.03	−0.09	−0.04	**0.04**	0	Population density-driven

The significant pc score is in bold font.

stronger development synergies based on complementarity and collaboration at the city cluster scale and have driven the YRDUA to become one of the most developed urban regions in the world today.

4.2. Four typical types of urban ECC driving patterns in the YRDUA

4.2.1. Urban expansion-driven pattern:

The urban expansion-driving cities, which indicates that the ECCI of cities is affected by the urban expansion process, are mainly distributed around Nanjing city in AH and JS. In the process of urbanization in industrialization, not only was the huge demand for construction land led by the increasing population inflow and economic development, but the expansion of urban construction land also led to land use structure change, which might lead to the reduction of cultivated land and the loss of vegetation cover at the same time (Li et al., 2020; Luo et al., 2021). While the EF increases, the land productivity also gradually fluctuates, resulting in an imbalance between the supply and demand of BC. Taking Yangzhou, the most typical urban expansion-driving city, as an example, the urban expansion-driving type was analyzed.

The urbanization rate of Yangzhou in 2015 reached 62.8%, compared with 41% in 2000, and there was a 21.8% increase in 15 years. The built-up area was 238 km^2 in 2015, and the cultivated land area was 295,120 ha, which was 20,000 ha lower than that in 2000. This result demonstrated the expansion of construction land and the encroachment of green land, including cultivated land. During the 15 years, there was a more serious overloading area in Yangzhou (Figs. 3 and A1), but the ECCI in Yangzhou was overall lower than that in southern JS, such as Suzhou and Wuxi. It is speculated that under the joint influence of the increase in the light index and the decrease in the NDVI, the mean value of the NDVI in Yangzhou was approximately 0.7, where the slope of the driving curve was the most significant (Fig. 5b and c). Hence, the ECCI would show an increasing trend, where the vegetation is destroyed by construction land expansion. In addition, the mean "light intensity" was 0.32, and the ECCI fell rapidly while the light intensity increased with the urbanization process. Therefore, in the past 15 years, there has been no serious ECCI increase or ecological degradation in Yangzhou compared with other cities in JS. Since 2015, there has been a recovery of cultivated land to some degree, and the expansion of construction land has gradually slowed. It could be predicted that the ECCI in Yangzhou will show a downward trend in the future with the high-quality urbanization process.

4.2.2. Green economy-driven pattern

Green economy-driving cities, showing that regional ECCI is mainly driven by how green the urban economic development is, are scattered among the three provinces. There are different development strategies in the process of economic development. Some cities sacrifice the environment and resources to maintain high-speed economic development; some cities develop labor-intensive industries, which also bring huge population pressure; and other cities develop high-tech industries, which consume fewer resources and are more sustainable (Kasztelan, 2017; Loiseau et al., 2016). In this study, the ECCI in green economy-driving cities mainly drives "GDP" rather than "carbon emissions". If the driving effect curve of GDP is positive, the economic development of this city is not green and sustainable; otherwise, it is green economic development.

Huaibei is a typical green economy-driving city whose driving effect curve of "GDP" is significantly positive (Fig. 5d), indicating that the ECCI will increase with rapid economic development in Huaibei. The GDP of Huaibei increased from 10.3 billion CNY in 2000 to 76 billion CNY in 2015 and reached 107 billion CNY in 2019. As shown in Fig. 3, with economic development, when the average local GDP exceeds 50 million CNY per km^2, the restrictive effect of GDP on ECCI gradually decreases. In 2015, the average GDP of Huaibei was currently close to 20 million CNY per km^2, indicating that the economic development of Huaibei still had a significant impact on ECCI. In the past 20 years, the per capita ECCI of Huaibei increased rapidly from 2000 to 2015 (Figs. 3 and A1), which also confirms the trend of ecological deterioration with the growth of GDP under this driving pattern. Therefore, Huaibei should push for green growth to accelerate investments and innovations that will underpin sustainable development and provide new economic opportunities in the future (Kasztelan, 2017).

4.2.3. Industrial structure-driven pattern:

The ECCI in industrial structure-driving cities, which are mainly distributed in northern AH and northern JS, is driven by the urban industrial structure. Different industries place different pressures on the ecology (Costantini et al., 2017). For example, the secondary industry usually places greater pressure on the environment, consuming more resources with more pollutant emissions, and it is generally believed that the tertiary industry is cleaner, greener, and more sustainable (Li and Pan, 2013). The industrial structure of AH in 2000 was OV1, OV2, and OV3, which accounted for 58.5%, 17%, and 24.5%, respectively. In the following 20 years, OV2 grew quickly. In 2010, OV2 exceeded half of the total GDP in AH. In 2019, the industrial structure in AH accounted for 7.8%, 41.4% and 50.8%, respectively. Wuhu, the most typical heavy industry city in AH, is taken as an example to analyze the industrial structure-driving pattern.

The industrial structure in 2015 in Wuhu was as follows: OV1 was 12.04 billion CNY, accounting for 4.9%, OV2 was 140.56 billion CNY, accounting for 57.2%, and OV3 was 93.13 billion CNY, accounting for 37.9%. As shown in Fig. 5e–g, the driving effect curves of OV2 and OV3 in Wuhu are positive and negative, respectively. In 2015, OV1, OV2, and OV3 per land area in Wuhu were 2 million CNY per km^2, 11 million CNY per $km^{2,}$ and 7 million CNY per $km^{2,}$ respectively. Therefore, in the past 20 years, with the increase in OV1, the ECCI has increased slightly (Figs. 3 and A1). While the rise of OV2 would lead to a significant increase in ECCI in the past, in the future, the increase of ECCI will slow down, which could be proven based on the relatively stable ECCI variation between 2015 and 2019 (Fig. A1). As OV3 increases, ECCI will show a more significant downward trend. In Wuhu and even in AH, the growth of OV2 was significantly faster than that of OV3, so the ECCI still showed an upward trend from 2000 to 2015 (Wu et al., 2021), and there was a more serious overloading area in AH.

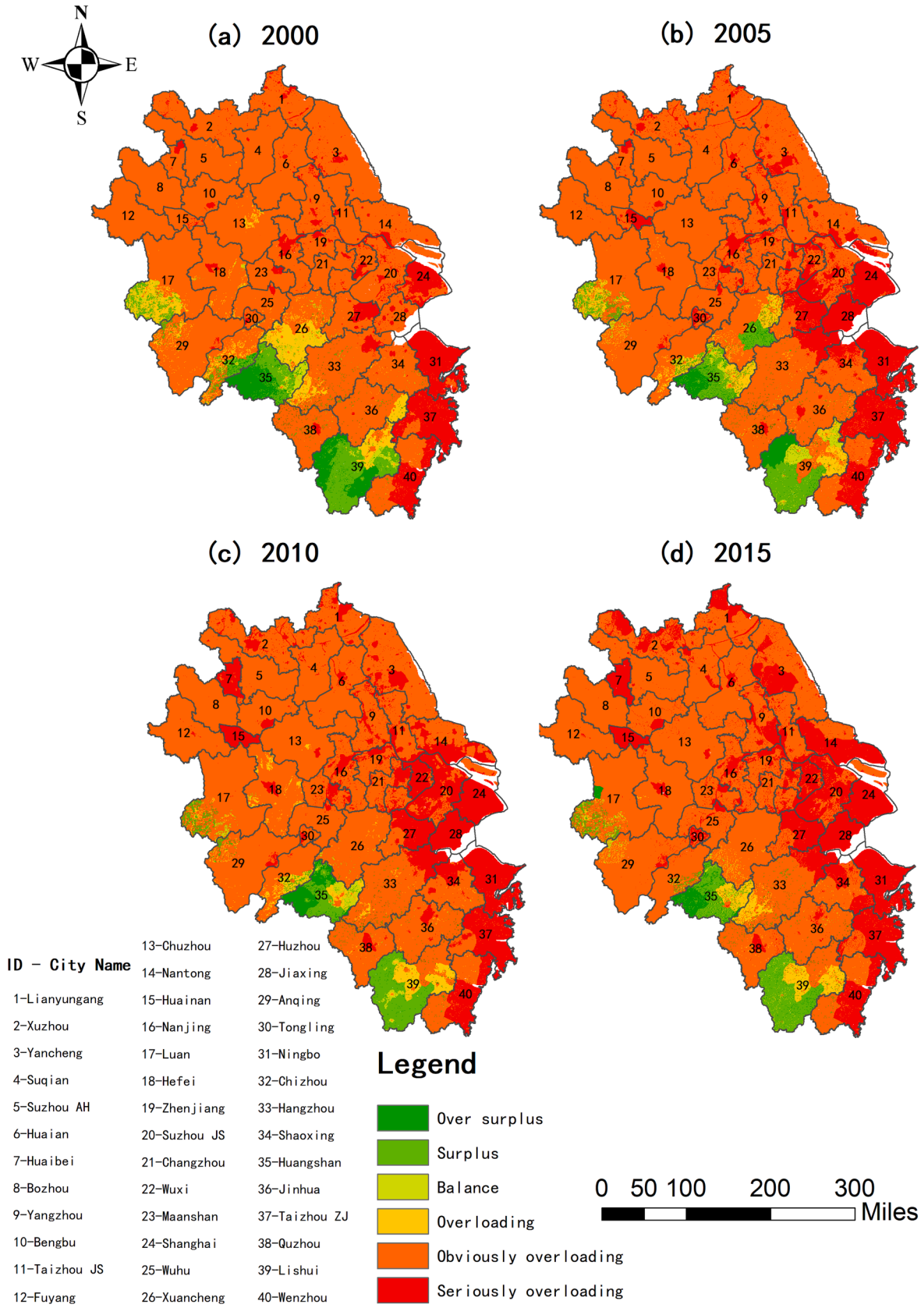

Fig. 4. ECCI spatial distribution of the YRDUA from 2000 to 2015.

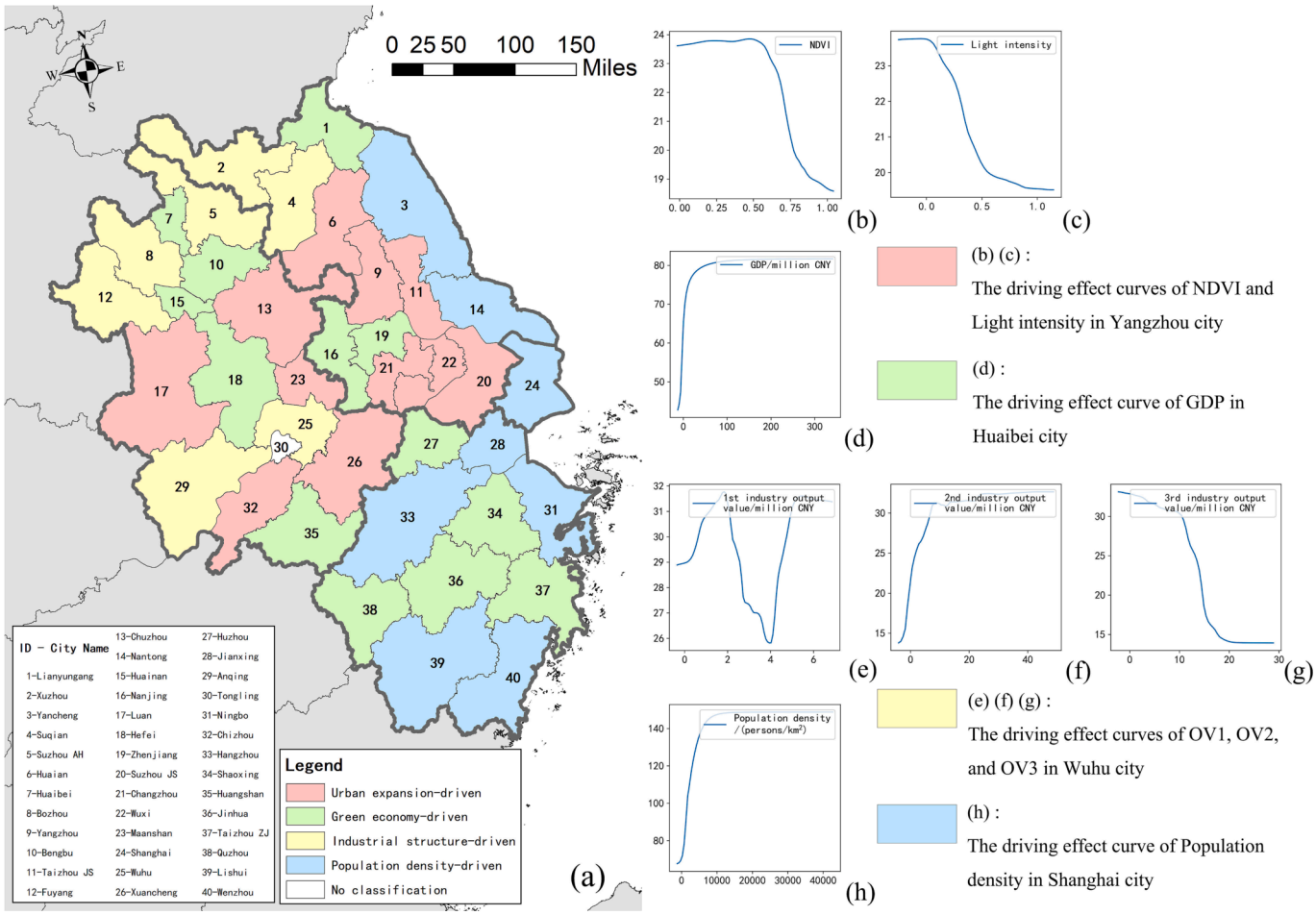

Fig. 5. (a): The distribution of the classification of urban ecological driving patterns; (b) (c): The driving effect curves of NDVI and light intensity in Yangzhou, which is a typical urban expansion-driving city; (d): The driving effect curve of GDP in Huaibei, which is a typical green economy-driving city; (e) (f) (g): The driving effect curve of OV1, OV2, and OV3 in Wuhu, which is a typical industrial structure-driving city; (h) The driving effect curve of population density in Shanghai, which is a typical population density-driving city.

4.2.4. Population density-driven model:

The population is the most essential feature affecting ECCI. The population density is directly related to the pressure on the ecological environment and the acquisition of natural resources by humans. Population density-driving cities are mainly distributed in the coastal areas of the YRDUA and are the main driving patterns in ZJ. In population density-driving cities, "Population density" is a relatively single driving feature for urban ECCI, and its DI is significantly higher than others. It is speculated that the industrial structure and land use structure of population density-driving cities are relatively stable and single, and a higher population leads to more human activities and ecological exploitation, so "Population density" became the most important factor affecting the urban ecological carrying status (Li et al., 2017). Taking Shanghai as an example, the DI of the other 10 features are all not significant, which means that the ECCI in Shanghai has a strong correlation with "Population density". The population density of Shanghai in 2015 was 3,830 persons/km^2. With the increase in population density, the ECCI increase rapidly, and there is still a long distance from the stationary point in the driving effect curve where the population density is nearly 10,000 (Fig. 5h). Therefore, in the future, the control of population density is still the most effective measure for ecological restoration in Shanghai and even other high-density population areas.

4.3. Sustainable development countermeasures in the YRDUA

According to the results of the spatial distribution of urban ecological driving patterns and the spatial differences of ECC in the YRDUA, different, regional, more rational, and more effective sustainable development countermeasures were proposed in JS, AH, Shanghai, and ZJ.

4.3.1. Optimizing the industrial structure and improving the greening of the economy: two important directions to guarantee regional ECC in JS and AH

There are mainly three types of urban ecological driving patterns in AH and JS, i.e., urban expansion-driving pattern, green economy-driving pattern, and industrial structure-driving pattern, except Yancheng and Nantong, which are coastal cities in JS (population density-driving type). Cities in northern Anhui and northern Jiangsu are mainly industrial structure-driving type where the ECCI during the 15 years was relatively lower than that of southern JS, indicating relatively low ecological pressure. Hence, they should vigorously develop tertiary industry and control the proportion of secondary industry at the same time to optimize the industrial structure. In addition, the urban expansion-driving cities in southern JS, central JS, and AN should strictly control the speed of urbanization and urban construction and stop the "great leap forward" of urbanization and urban expansion, which would be more conducive to ecological restoration than other measures, rather than just pursuing the urbanization rate, but should gradually achieve the full urbanization goal in the long term. At the same time, urban construction areas should not expand at the expense of ecological land, especially in Changzhou, Wuxi, and Suzhou in southern Jiangsu, where the ECCI has reached a serious overloading level.

Nanjing, Hefei, and their neighboring cities, which are the green economy-driving type, should pay more attention to the consumption of resources and pollution emissions in the process of economic development, which can also be achieved by industrial restructuring, optimization, and upgrading or even banning industries and factories with serious pollution and low resource utilization.

In the future, JS and AH should focus on industrial structure optimization, environmentally friendly industry development, management of traditional industries and resource-consuming industries, and combating vegetation degradation led by urban expansion.

4.3.2. Controlling population density and saving resource costs are the key goals for regional maintenance of ECC in Shanghai and ZJ

There are only two types of ecological driving patterns in Shanghai and ZJ, i.e.,the green economy-driving pattern and the population density-driving pattern. Therefore, for the densely populated area in Shanghai and ZJ, the imbalance of ecological supply and demand caused by high population density could be alleviated through the expansion of the construction area, while for mega-cities such as Shanghai and Hangzhou, the government should alleviate the pressure of the urban population through industrial relocation and settlement restrictions.

Cities in central ZJ, which are mainly the green economy-driving type, should pay more attention to the resource and environmental costs of economic development while making full efforts to economic development, reduce the excessive energy consumption caused by development, and support the technological innovation and development of the high-tech industry to promote energy conservation and emission reduction in production and life.

5. Conclusion:

In this study, we constructed multiple artificial neural networks for 40 cities in the YRDUA to approximate the ecological carrying capacity supply and demand balance index (ECCI) in 2015 using 11 socioeconomic factors. Then, we disassembled the models and analyzed the ecological driving effect curves of each city. Driving intensity (DI) was introduced to define how strongly ECCI is driven by the feature. We found that “Population density” was the most significant feature driving ECCI with the highest average DI value, while “GDP”, “Output value of the 1st”, “Output value of the 2nd”, and “Output value of the 3rd” were also relatively significant. According to the DI, we classified the YRDUA cities, and 4 ecological driving patterns were obtained, i.e., urban expansion-driving pattern, green economy-driving pattern, industrial structure-driving pattern, and population density-driving pattern. Finally, we analyzed different ecological driving patterns based on their spatial distribution and the spatial–temporal pattern of the ECCI from 2000 to 2015. The results showed that there would be two main measures for sustainable development in Jiangsu province and Anhui province: one focus on industrial structure optimization, and the other focuses on urban built-up area management and vegetation restoration. In addition, there will also be two main measures in Shanghai city and Zhejiang province: one is to reduce the resource and environmental costs of economic development, and the other is population control.

This research provided a new idea and framework to solve the problem of how ecological systems respond to socioeconomic systems, and a reference for regional sustainable development policymaking. However, it is also necessary for scholars to further improve the research related to the temporal change in ecological driving patterns in the same area and verify the “inflection point” and “stagnation point” of driving curves.

CRediT authorship contribution statement

Chang Liu: Conceptualization, Methodology, Software, Validation, Formal analysis, Data curation, Writing – original draft, Visualization. **Tianhua Ni:** Conceptualization, Investigation, Resources, Writing – review & editing, Supervision, Project administration, Funding acquisition.

Declaration of Competing Interest

The authors declare that they have no known competing financial interests or personal relationships that could have appeared to influence the work reported in this paper.

Data availability

Data will be made available on request.

Acknowledgments

The authors thank Dr. Yi Qi for his valuable comments and discussion.

Funding

This work was supported by the Department of Science and Technology of Jiangsu Province (http://std.jiangsu.gov.cn/) [grant number 201904] to Tianhua Ni.

Appendix A. Supplementary data

Supplementary data to this article can be found online at https://doi.org/10.1016/j.ecolind.2023.110231.

References

Abdi, H., Williams, L.J., 2010. Principal component analysis: principal component analysis. WIREs. Comp. Stat. 2, 433–459. https://doi.org/10.1002/wics.101.

Ahmed, Z., Wang, Z., Mahmood, F., Hafeez, M., Ali, N., 2019. Does globalization increase the ecological footprint? Empirical evidence from Malaysia. Environ Sci. Pollut. Res. 26, 18565–18582. https://doi.org/10.1007/s11356-019-05224-9.

Ahmed, Z., Zhang, B., Cary, M., 2021. Linking economic globalization, economic growth, financial development, and ecological footprint: Evidence from symmetric and asymmetric ARDL. Ecol. Indic. 121, 107060 https://doi.org/10.1016/j.ecolind.2020.107060.

Annan-Diab, F., Molinari, C., 2017. Interdisciplinarity: practical approach to advancing education for sustainability and for the Sustainable Development Goals. The Int. J. Manag. Educ. 15, 73–83. https://doi.org/10.1016/j.ijme.2017.03.006.

Baabou, W., Grunewald, N., Ouellet-Plamondon, C., Gressot, M., Galli, A., 2017. The Ecological Footprint of Mediterranean cities: awareness creation and policy implications. Environ. Sci. Policy 69, 94–104. https://doi.org/10.1016/j.envsci.2016.12.013.

Bai, Y., Zeng, H., Wei, J., Zhang, W., Zhao, H., 2008. Optimization of ecological footprint model based on environmental pollution accounts: a case study in Pearl River Delta urban agglomeration. J. Appl. Ecol. 19, 1789–1796.

Balsalobre-Lorente, D., Gokmenoglu, K.K., Taspinar, N., Cantos-Cantos, J.M., 2019. An approach to the pollution haven and pollution halo hypotheses in MINT countries. Environ. Sci. Pollut. Res. 26, 23010–23026. https://doi.org/10.1007/s11356-019-05446-x.

Borucke, M., Moore, D., Cranston, G., Gracey, K., Iha, K., Larson, J., Lazarus, E., Morales, J.C., Wackernagel, M., Galli, A., 2013. Accounting for demand and supply of the biosphere’s regenerative capacity: the National Footprint Accounts’ underlying methodology and framework. Ecol. Indic. 24, 518–533. https://doi.org/10.1016/j.ecolind.2012.08.005.

Butlin, J., 1989. Our common future. By World commission on environment and development. (London, Oxford University Press, 1987, pp.383 £5.95.). J. Int. Dev. 1 (2), 284–287.

Cano-Orellana, A., Delgado-Cabeza, M., 2015. Local ecological footprint using Principal Component Analysis: A case study of localities in Andalusia (Spain). Ecol. Indic. 57, 573–579. https://doi.org/10.1016/j.ecolind.2015.03.014.

Chen, T., Feng, Z., Zhao, H., Wu, K., 2020a. Identification of ecosystem service bundles and driving factors in Beijing and its surrounding areas. Sci. Total Environ. 711, 134687 https://doi.org/10.1016/j.scitotenv.2019.134687.

Chen, Y., Lu, H., Li, J., Xia, J., 2020b. Effects of land use cover change on carbon emissions and ecosystem services in Chengyu urban agglomeration, China. Stoch. Environ. Res. Risk. Assess. 34, 1197–1215. https://doi.org/10.1007/s00477-020-01819-8.

Costantini, V., Crespi, F., Marin, G., Paglialunga, E., 2017. Eco-innovation, sustainable supply chains and environmental performance in European industries. J. Clean. Prod. 155, 141–154. https://doi.org/10.1016/j.jclepro.2016.09.038.

Čuček, L., Klemeš, J.J., Kravanja, Z., 2012. A Review of Footprint analysis tools for monitoring impacts on sustainability. J. Clean. Prod. 34, 9–20. https://doi.org/10.1016/j.jclepro.2012.02.036.
Danish, Ulucak, R., Khan, S.-D., 2020. Determinants of the ecological footprint: role of renewable energy, natural resources, and urbanization. Sustain. Cities Soc. 54, 101996.
Danish, wang, Z., 2019. Investigation of the ecological footprint's driving factors: What we learn from the experience of emerging economies. Sustain. Cities Soc. 49, 101626.
Destek, M.A., Sarkodie, S.A., 2019. Investigation of environmental Kuznets curve for ecological footprint: the role of energy and financial development. Sci. Total Environ. 650, 2483–2489. https://doi.org/10.1016/j.scitotenv.2018.10.017.
Dietz, T., Rosa, E.A., York, R., 2007. Driving the human ecological footprint. Front. Ecol. Environ. 5, 13–18. https://doi.org/10.1890/1540-9295(2007)5[13:DTHEF]2.0.CO;2.
Ewing, B.R., Hawkins, T.R., Wiedmann, T.O., Galli, A., Ertug Ercin, A., Weinzettel, J., Steen-Olsen, K., 2012. Integrating ecological and water footprint accounting in a multi-regional input–output framework. Ecol. Indic. 23, 1–8. https://doi.org/10.1016/j.ecolind.2012.02.025.
Galli, A., Wackernagel, M., Iha, K., Lazarus, E., 2014. Ecological footprint: implications for biodiversity. Biol. Conserv. 173, 121–132. https://doi.org/10.1016/j.biocon.2013.10.019.
Griggs, D., Stafford-Smith, M., Gaffney, O., Rockström, J., Öhman, M.C., Shyamsundar, P., Steffen, W., Glaser, G., Kanie, N., Noble, I., 2013. Sustainable development goals for people and planet. Nature 495, 305–307. https://doi.org/10.1038/495305a.
Han, X., Zhou, Y.I., Wang, S.X., Liu, R., Yao, Y., 2012. GDP spatialization in China based on nighttime imagery. Geogr. Inf. Sci. 14, 128–136.
Hodgkinson, T., Andresen, M.A., 2019. Changing spatial patterns of residential burglary and the crime drop: the need for spatial data signatures. J. Crim. Justice 61, 90–100. https://doi.org/10.1016/j.jcrimjus.2019.04.003.
Hong, S., Guo, Q., Li, D., 2020. Spatiotemporal dynamics of ecological supply and demand based on ecological footprint theory. Resour. Sci. 42, 980–990. https://doi.org/10.18402/resci.2020.05.15.
Hong, L.i., Pei Dong, Z., Chunyu, H., Gang, W., 2007. Evaluating the effects of embodied energy in international trade on ecological footprint in China. Ecol. Econ. 62, 136–148. https://doi.org/10.1016/j.ecolecon.2006.06.007.
Johannesson, S.E., Heinonen, J., Davidsdottir, B., 2020. Data accuracy in Ecological Footprint's carbon footprint. Ecol. Indic. 111, 105983 https://doi.org/10.1016/j.ecolind.2019.105983.
Kasztelan, A., 2017. Green growth, green economy and sustainable development: terminological and relational discourse. Prague Econ. Pap. 26, 487–499. https://doi.org/10.18267/j.pep.626.
LeCun, Y., Bengio, Y., Hinton, G., 2015. Deep learning. Nature 521, 436–444. https://doi.org/10.1038/nature14539.
Lee, S.-I., Celik, S., Logsdon, B.A., Lundberg, S.M., Martins, T.J., Oehler, V.G., Estey, E.H., Miller, C.P., Chien, S., Dai, J., Saxena, A., Blau, C.A., Becker, P.S., 2018. A machine learning approach to integrate big data for precision medicine in acute myeloid leukemia. Nat. Commun. 9, 42. https://doi.org/10.1038/s41467-017-02465-5.
Li, X., Pan, J. (Eds.), 2013. China Green Development Index Report 2011. Springer Berlin Heidelberg, Berlin, Heidelberg. https://doi.org/10.1007/978-3-642-31597-8.
Li, J., Pu, R., Gong, H., Luo, X., Ye, M., Feng, B., 2017. Evolution characteristics of landscape ecological risk patterns in coastal zones in Zhejiang Province, China. Sustainability 9, 584. https://doi.org/10.3390/su9040584.
Li, D., Wu, S., Liang, Z., Li, S., 2020. The impacts of urbanization and climate change on urban vegetation dynamics in China. Urban. For. Urban. Green. 54, 126764 https://doi.org/10.1016/j.ufug.2020.126764.
Lin, D., Hanscom, L., Murthy, A., Galli, A., Evans, M., Neill, E., Mancini, M., Martindill, J., Medouar, F.-Z., Huang, S., Wackernagel, M., 2018. Ecological footprint accounting for countries: updates and results of the national footprint accounts, 2012–2018. Resources 7, 58. https://doi.org/10.3390/resources7030058.
Liu, D., Feng, Z., Yang, Y., You, Z., 2011. Spatial patterns of ecological carrying capacity supply-demand balance in China at county level. J. Geogr. Sci. 21, 833–844. https://doi.org/10.1007/s11442-011-0883-0.
Liu, M., Li, W., Zahng, D., Su, N., 2015. The calculation of equivalence factor for ecological footprints in China: a methodological note. Front. Environ. Sci. Eng. 9, 1015–1024. https://doi.org/10.1007/s11783-014-0670-0.
Liu, M., Liu, C., Pei, X., Zhang, S., Ge, X., Zhang, H., Li, Y., 2021. Sustainable risk assessment of resource industry at provincial level in China. Sustainability. 13, 4191. https://doi.org/10.3390/su13084191.
Liu, C., Qi, Y.i., Wang, Z., Yu, J., Li, S., Yao, H., Ni, T., Xue, B., 2020a. Deep learning: to better understand how human activities affect the value of ecosystem services—A case study of Nanjing. PLoS ONE 15 (10), e0238789.
Liu, J., Zhao, D., Mao, G., Cui, W., Chen, H., Yang, H., 2020b. Environmental sustainability of water footprint in Mainland China. Geogr. Sustain. 1, 8–17. https://doi.org/10.1016/j.geosus.2020.02.002.
Loiseau, E., Saikku, L., Antikainen, R., Droste, N., Hansjürgens, B., Pitkänen, K., Leskinen, P., Kuikman, P., Thomsen, M., 2016. Green economy and related concepts: an overview. J. Clean. Prod. 139, 361–371. https://doi.org/10.1016/j.jclepro.2016.08.024.
Lundberg, S.M., Lee, S.-I., 2017. A Unified Approach to Interpreting Model Predictions. Advances in Neural Information Processing Systems. Curran Associates Inc.
Luo, Y., Sun, W., Yang, K., Zhao, L., 2021. China urbanization process induced vegetation degradation and improvement in recent 20 years. Cities 114, 103207. https://doi.org/10.1016/j.cities.2021.103207.
Monfreda, C., Wackernagel, M., Deumling, D., 2004. Establishing national natural capital accounts based on detailed Ecological Footprint and biological capacity assessments. Land Use Policy 21, 231–246. https://doi.org/10.1016/j.landusepol.2003.10.009.
Moore, D.W., Booth, P., Alix, A., Apitz, S.E., Forrow, D., Huber-Sannwald, E., Jayasundara, N., 2017. Application of ecosystem services in natural resource management decision making. Integr. Environ. Assess. Manag. 13, 74–84. https://doi.org/10.1002/ieam.1838.
Niccolucci, V., Bastianoni, S., Tiezzi, E.B.P., Wackernagel, M., Marchettini, N., 2009. How deep is the footprint? A 3D representation. Ecol. Modell. 220, 2819–2823. https://doi.org/10.1016/j.ecolmodel.2009.07.018.
Olawumi, T.O., Chan, D.W.M., 2018. A scientometric review of global research on sustainability and sustainable development. J. Clean. Prod. 183, 231–250. https://doi.org/10.1016/j.jclepro.2018.02.162.
Omoke, P.C., Nwani, C., Effiong, E.L., Evbuomwan, O.O., Emenekwe, C.C., 2020. The impact of financial development on carbon, non-carbon, and total ecological footprint in Nigeria: new evidence from asymmetric dynamic analysis. Environ. Sci. Pollut. Res. 27, 21628–21646. https://doi.org/10.1007/s11356-020-08382-3.
Pei, F., Zhong, R., Liu, L.-A., Qiao, Y., 2021. Decoupling the relationships between carbon footprint and economic growth within an urban agglomeration—A case study of the yangtze river delta in China. Land 10, 923. https://doi.org/10.3390/land10090923.
Qi, Y., Chodron Drolma, S., Zhang, X., Liang, J., Jiang, H., Xu, J., Ni, T., 2020. An investigation of the visual features of urban street vitality using a convolutional neural network. Geo. Spat. Inf. Sci. 23, 341–351. https://doi.org/10.1080/10095020.2020.1847002.
Rees, W.E., 1996. Revisiting carrying capacity: area-based indicators of sustainability. Popul. Environ. 17, 195–215. https://doi.org/10.1007/BF02208489.
Reichstein, M., Camps-Valls, G., Stevens, B., Jung, M., Denzler, J., Carvalhais, N., Prabhat, 2019. Deep learning and process understanding for data-driven Earth system science. Nature 566, 195–204. https://doi.org/10.1038/s41586-019-0912-1.
Sarkodie, S.A., 2021. Environmental performance, biocapacity, carbon & ecological footprint of nations: Drivers, trends and mitigation options. Sci. Total Environ. 751, 141912 https://doi.org/10.1016/j.scitotenv.2020.141912.
Stojić, A., Stanić, N., Vuković, G., Stanišić, S., Perišić, M., Šoštarić, A., Lazić, L., 2019. Explainable extreme gradient boosting tree-based prediction of toluene, ethylbenzene and xylene wet deposition. Sci. Total Environ. 653, 140–147. https://doi.org/10.1016/j.scitotenv.2018.10.368.
Syrovátka, M., 2020. On sustainability interpretations of the Ecological Footprint. Ecol. Econ. 169, 106543 https://doi.org/10.1016/j.ecolecon.2019.106543.
Sze, V., Chen, Y.-H., Yang, T.-J., Emer, J.S., 2017. Efficient processing of deep neural networks: a tutorial and survey. Proc. IEEE. 105, 2295–2329. https://doi.org/10.1109/JPROC.2017.2761740.
Wackernagel, M., Onisto, L., Bello, P., Callejas Linares, A., Susana López Falfán, I., Méndez García, J., Isabel Suárez Guerrero, A., Guadalupe Suárez Guerrero, M., 1999.
Wackernagel, M., Onisto, L., Bello, P., Callejas Linares, A., Susana López Falfán, I., Méndez García, J., Isabel Suárez Guerrero, A., Guadalupe Suárez Guerrero, M.a., 1999b. National natural capital accounting with the ecological footprint concept. Ecol. Econ. 29 (3), 375–390.
Wackernagel, M., Rees, W.E., 1997. Perceptual and structural barriers to investing in natural capital: economics from an ecological footprint perspective. Ecol. Econ. 20, 3–24. https://doi.org/10.1016/S0921-8009(96)00077-8.
Wang, J., Dong, K., 2019. What drives environmental degradation? Evidence from 14 sub-saharan African countries. Sci. Total Environ. 656, 165–173. https://doi.org/10.1016/j.scitotenv.2018.11.354.
Wang, C., Qi, Y., Zhu, G., 2020a. Deep learning for predicting the occurrence of cardiopulmonary diseases in Nanjing. China. Chemosphere 257, 127176. https://doi.org/10.1016/j.chemosphere.2020.127176.
Wang, C., Feng, L., Qi, Y., 2021. Explainable deep learning predictions for illness risk of mental disorders in Nanjing. China. Environ. Res. 202, 111740 https://doi.org/10.1016/j.envres.2021.111740.
Wang, J., Huang, X., Zhong, T., Chen, Z., 2013. Climate change impacts and adaptation for saline agriculture in north Jiangsu Province, China. Environ. Sci. Policy 25, 83–93. https://doi.org/10.1016/j.envsci.2012.07.011.
Wang, L., Zhang, L., Zhu, M., Qi, X., Yi, Z., 2020b. Automatic diagnosis for thyroid nodules in ultrasound images by deep neural networks. Med. Image Anal. 61, 101665 https://doi.org/10.1016/j.media.2020.101665.
Williams, E., Wackernagel, M., 1998. Our ecological footprint: reducing human impact on earth (Vol. 9). New society publishers, Gabriola, BC, Canada.
Wu, C., Wei, Y.D., Huang, X., Chen, B., 2017. Economic transition, spatial development and urban land use efficiency in the Yangtze River Delta, China. Habitat Int. 63, 67–78. https://doi.org/10.1016/j.habitatint.2017.03.012.
Wu, W., Zhang, T., Xie, X., Huang, Z., 2021. Regional low carbon development pathways for the Yangtze River Delta region in China. Energy Policy 151, 112172. https://doi.org/10.1016/j.enpol.2021.112172.
Yang, Y., Fan, M., 2019. Analysis of the spatial-temporal differences and fairness of the regional energy ecological footprint of the Silk Road Economic Belt (China Section). J. Clean. Prod. 215, 1246–1261. https://doi.org/10.1016/j.jclepro.2019.01.170.
Yang, Y., Ling, S., Zhang, T., Yao, C., 2018. Three-dimensional ecological footprint assessment for ecologically sensitive areas: A case study of the Southern Qin Ling piedmont in Shaanxi, China. J. Clean. Prod. 194, 540–553. https://doi.org/10.1016/j.jclepro.2018.05.132.
Yang, Y., Lu, H., Liang, D., Chen, Y., Tian, P., Xia, J., Wang, H., Lei, X., 2022. Ecological sustainability and its driving factor of urban agglomerations in the Yangtze River Economic Belt based on three-dimensional ecological footprint analysis. J. Clean. Prod. 330, 129802 https://doi.org/10.1016/j.jclepro.2021.129802.
Zhang, L., Godil, D.I., Bibi, M., Khan, M.K., Sarwat, S., Anser, M.K., 2021. Caring for the environment: how human capital, natural resources, and economic growth interact

with environmental degradation in Pakistan? A dynamic ARDL approach. Sci. Total Environ. 774, 145553 https://doi.org/10.1016/j.scitotenv.2021.145553.
Zhen, F., Cao, Y., Qin, X., Wang, B., 2017. Delineation of an urban agglomeration boundary based on Sina Weibo microblog 'check-in' data: a case study of the Yangtze River Delta. Cities 60, 180–191. https://doi.org/10.1016/j.cities.2016.08.014.
Zongguang, L.I., Deyong, H.U., Jihe, L.I., Jian, C.E.N., 2016. Simulation and spatialization of GDP in poverty areas based on night light imagery. Remote Sens. Nat. Res. 168–174 https://doi.org/10.6046/gtzyyg.2016.02.26.